Numerical Approach to Maneuver Design and Feasibility Evaluation for the Autonomy of Airship

Duraisamy Gobiha and Nandan K. Sinha

1 Introduction

Feasible or implementable maneuver design and evaluation is an indispensable area of research in the aerospace control fraternity. Literature rarely emphasizes the feasibility of the chosen desired trajectory or path. Among the ones that contemplate feasibility, optimization is the most prevalent approach, with one being an opportune byproduct of the other [1]. Optimization-based control design like model predictive control (MPC) when implemented on real-time systems requires strictly guaranteed convergence and heavy computational resources mainly for high-performance aerospace applications. Besides, such integration of optimization and control questions the reliability of controls in real-time implementation with modeled and unmodeled uncertainties, process, measurement noise, etc. [1].

Most practical applications merely need a feasible solution rather than an optimal one. The recent introduction of computational guidance and control [1, 2] further provokes the importance of an alternate methodology to obtain feasible solutions. But there are very few non-optimal feasible maneuver design techniques discussed in the literature. Trajectory generation based on analytically solving trim solutions is proposed in [3]. Besides being cumbersome, this method does not give explicit solutions and does not contemplate on stability. In [4], appropriate control inputs pertaining to the reference trajectory are obtained by solving the system's dynamical equations. This is just a validation procedure and relies on trial-and-error for obtaining a feasible reference trajectory.

Maneuver design based on bifurcation analysis has been attempted in [5] using continuation algorithm, AUTO2000. This work generates feasible solutions and uses two trim points between which state variables are switched, to achieve the maneuver.

D. Gobiha (✉) · N. K. Sinha
Department of Aerospace Engineering, Indian Institute of Technology Madras,
Chennai 600036, India
e-mail: gobiha@yahoo.com

This method does not perceive trajectory design as a whole and continuation algorithms using AUTO2000 are highly dependent on the initial conditions and are computationally demanding. This significantly limits the applicability of this methodology. But with the recent development of MATLAB® embedded continuation algorithms like MATCONT [6], a direct continuation methodology for constrained system analysis has been proposed which significantly overcomes the complexity of the continuation procedure [7].

This work uses the bifurcation-based continuation technique to compute feasible solutions for different maneuvers regarded for autonomous operations of stratospheric airship. The computed solutions take into account the complete dynamics of the considered airship model with its state and control constraints. Some of the challenging aspects of stratospheric airship like ascending, descending, and hovering with a minimal lateral excursion are interpreted and validated.

The paper is structured as follows. Section 2 presents the mathematical modeling of the considered six degrees-of-freedom stratospheric airship model. Section 3 elaborates the numerical description of bifurcation analysis for multi-input multi-output dynamical systems. Maneuver design for various flight conditions like a level straight, level turn, hover, ascend, and descend is discussed in Sect. 4. Simulation for the validation of formulated maneuvers is carried out in Sect. 5. Section 6 concludes the paper.

2   6-DoF Aircraft Equations of Motion

This work considers an airship at an operational altitude of 21 km. Such airships are called high altitude or stratospheric airships as they operate in the stratospheric regime of the atmosphere. Airships in this regime face minimal intrusions from other aerial vehicles and provide better remote sensing due to their proximity to the ground. Reusability along with its greener, cheaper and quieter operations, makes stratospheric airship an effective platform for surveillance, atmospheric measurements, disaster management, and space tourism. Though real-time implementation of low altitude airships is uncomplicated, mainly in ascend and descend phases, stratospheric airships have strategic advantages like low magnitude wind speed as inferred from the global atmospheric wind profile [8] and extensive geographic area coverage, which serves enormous applications.

The considered airship is Gertler shaped with a hull filled with helium gas and ballonets filled with air to regulate the internal pressure of airship. A cruciform tail configuration at the rear serves as the control actuator for the airship. The fin deflections of four arms are characterized as elevator (δ_e), aileron (δ_a), and rudder (δ_r) angles as illustrated in Fig. 1 for the ease of incorporation in aerodynamic model of the airship. Resultant of fin deflections that generates pitch, yaw, and roll forces and moments are defined as elevator (δ_e), aileron (δ_a), and rudder (δ_r) angles as tabulated in Eqs. (1)–(3),

Fig. 1 Rear view of tail configuration
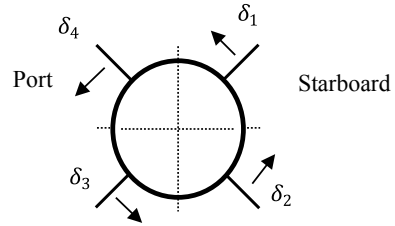
$$\delta_e = \frac{\delta_1 + \delta_2 - \delta_3 - \delta_4}{4} \tag{1}$$

$$\delta_r = \frac{-\delta_1 + \delta_2 + \delta_3 - \delta_4}{4} \tag{2}$$

$$\delta_a = \frac{\delta_1 + \delta_2 + \delta_3 + \delta_4}{4} \tag{3}$$

Structural analysis, stability, and control derivatives and inertial values of the airship were extensively evaluated in [9]. Six degrees-of-freedom modeling of airship should consider inertial, aerodynamic, gravitational, buoyant, and propulsive forces. In this work, equations of motion of airship are derived with components along the wind axes frame with origin, o at the center of volume (CV). Airship equations of motions are similar to that of aircraft except for the influence of buoyant force on translational and rotational dynamic equations. Buoyant force along with virtual mass and inertia terms has a significant influence on the dynamic equations, whereas translational and rotational kinematic equations are the same as that of aircraft, as tabulated in Eqs. (4)–(9) [10]

$$\begin{aligned}
\dot{x}_E = {} & V \cos\alpha \cos\beta (\cos\psi \cos\theta) \\
& + V \sin\beta (\cos\psi \sin\theta \sin\phi - \sin\psi \cos\phi) \\
& + V \sin\alpha \cos\beta (\cos\psi \sin\theta \cos\phi + \sin\psi \sin\phi)
\end{aligned} \tag{4}$$

$$\begin{aligned}
\dot{y}_E = {} & V \cos\alpha \cos\beta (\sin\psi \cos\theta) \\
& + V \sin\beta (\sin\psi \sin\theta \sin\phi + \cos\psi \cos\phi) \\
& + V \sin\alpha \cos\beta (\sin\psi \sin\theta \cos\phi - \cos\psi \sin\phi)
\end{aligned} \tag{5}$$

$$\begin{aligned}
\dot{z}_E = {} & V \cos\alpha \cos\beta (-\sin\theta) + V \sin\beta (\cos\theta \sin\phi) \\
& + V \sin\alpha \cos\beta (\cos\theta \cos\phi)
\end{aligned} \tag{6}$$

$$\dot{\phi} = p + q \sin\phi \tan\theta + r \cos\phi \tan\theta \tag{7}$$

$$\dot{\theta} = q \cos \phi - r \sin \phi \tag{8}$$

$$\dot{\psi} = \sec \theta (q \sin \phi + r \cos \phi) \tag{9}$$

2.1 Buoyant and Gravitational Terms

The buoyant force acts along $-Z_E$ axis, whereas gravitational force acts along $+Z_E$ axis. On using the transformation matrix as contemplated in [10], buoyant and gravitational forces (F_{bg}) are transformed from inertial axes system to wind axes system.

$$F_{bg} = \begin{bmatrix} 0 \\ 0 \\ mg - B \end{bmatrix}_E = \begin{bmatrix} -(mg - B) \sin \gamma \\ (mg - B) \cos \gamma \sin \mu \\ (mg - B) \cos \gamma \cos \mu \end{bmatrix}_W \tag{10}$$

Moment generated on the airship due to buoyant and gravitational terms (M_{bg}) is illustrated in [8].

$$M_{bg} = \begin{bmatrix} -(mga_z + Bb_z) \sin \phi \cos \theta \\ -(mga_z + Bb_z) \sin \theta - (mga_x + Bb_x) \cos \phi \cos \theta \\ (mga_x + Bb_x) \sin \phi \cos \theta \end{bmatrix} \tag{11}$$

2.2 Aerodynamic and Control Terms

Aerodynamic and control force and moment act along the stability axes of the system. Thus on transforming it in wind axis frame, aerodynamic force (F_a) is given by

$$F_a = \begin{bmatrix} -D \\ Y \\ -L \end{bmatrix}_S = \frac{1}{2} \rho V^2 S \begin{bmatrix} -C_D \cos \beta + C_Y \sin \beta \\ C_D \sin \beta + C_Y \cos \beta \\ -C_L \end{bmatrix}_W \tag{12}$$

Similarly, aerodynamic moment vector (M_a) is given by

$$M_a = \begin{bmatrix} \mathcal{L} \\ M \\ N \end{bmatrix} = \frac{1}{2} \rho V^2 S \begin{bmatrix} bC_l \\ cC_m \\ bC_n \end{bmatrix} \tag{13}$$

2.3 Propulsive Terms

The propulsive system consists of a symmetric pair of thrusters on the aft of CV. The thruster on the port and starboard sides of airship is represented by T_p and T_s, and they are inclined at an angle ζ_p and ζ_s, respectively. In this work, it is assumed that the direction of tilt angles and magnitude of thrust along both port and starboard sides are identical. The coordinates of both thrusters are (d_x, d_y, d_z) as shown in Fig. 2.

The propulsive force along body axes frame is

$$F_p = \begin{bmatrix} T_s \cos \zeta_s + T_p \cos \zeta_p \\ 0 \\ -(T_s \sin \zeta_s + T_p \sin \zeta_p) \end{bmatrix}_B = \begin{bmatrix} (T_s + T_p) \cos \zeta \\ 0 \\ -(T_s + T_p) \sin \zeta \end{bmatrix}_B \qquad (14)$$

On transforming the force from body to wind axes system, Eq. (14) becomes

$$F_p = \begin{bmatrix} (T_s + T_p) \cos \zeta \cos \alpha \cos \beta - (T_s + T_p) \sin \zeta \sin \alpha \cos \beta \\ -(T_s + T_p) \cos \zeta \cos \alpha \sin \beta + (T_s + T_p) \sin \zeta \sin \alpha \sin \beta \\ -(T_s + T_p) \cos \zeta \sin \alpha - (T_s + T_p) \sin \zeta \cos \alpha \end{bmatrix}_W \qquad (15)$$

Similarly, moment due to propulsive system (M_p) is given by
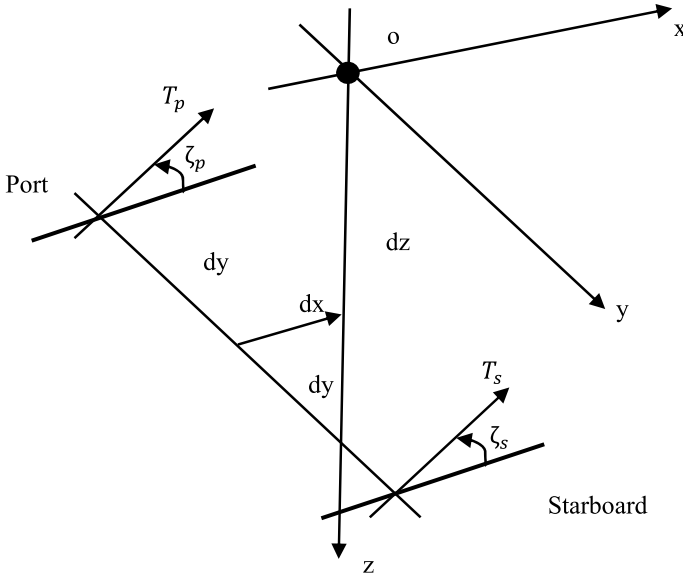
Fig. 2 Geometry of propulsive system

$$M_p = \begin{bmatrix} (T_p \sin \zeta_p - T_s \sin \zeta_s)d_y \\ T_p(d_z \cos \zeta_p - d_x \sin \zeta_p) + T_s(d_z \cos \zeta_s - d_x \sin \zeta_s) \\ (T_p \cos \zeta_p - T_s \cos \zeta_s)d_y \end{bmatrix}$$

$$= \begin{bmatrix} (T_p - T_s) \sin \zeta \, d_y \\ (T_p + T_s)(d_z \cos \zeta - d_x \sin \zeta) \\ (T_p - T_s) \cos \zeta \, d_y \end{bmatrix} \tag{16}$$

Assumptions that are incorporated based on design aspects of the airship are

(1) Symmetric about xz plane with both center of buoyancy (CB) and center of gravity (CG) in that plane, i.e., $a_y = b_y = 0$.
(2) CV coincides with CB, i.e., $a_x = a_z = 0$ and CB is above CV, i.e., $b_x = 0$.
(3) Thrusters are assumed to be positioned below CV, therefore, $d_x = 0$.
(4) This work also assumes non-differential thrust and angle, i.e., $T_s = T_p = T/2$ and $\zeta_s = \zeta_p = \zeta$.
(5) Neutral buoyancy is considered throughout the entire flight regime.
(6) Airship is considered an open system, with mass remaining constant and volume varying with the inflation and deflation of ballonets.

Based on these assumptions and the derived terms, Newton's second law of motion is applied to each degree-of-freedom [8]. Translational and rotational dynamic equations are subsequently arrived at and are presented in Eqs. (17)–(22).

$$\dot{p} = \left(\frac{J_y - J_z}{J_x}\right)qr + \left(\frac{J_{xz}}{J_x}\right)pq - \left(\frac{Bb_z}{J_x}\right)\sin\phi\cos\theta + \frac{1}{2J_x}\rho V^2 SbC_l \tag{17}$$

$$\dot{q} = \left(\frac{J_z - J_x}{J_y}\right)pr + \left(\frac{J_{xz}}{J_y}\right)(r^2 - p^2)$$
$$- \left(\frac{Bb_z}{J_y}\right)\sin\theta + \left(\frac{T}{J_y}\right)d_z \cos\zeta + \frac{1}{2J_y}\rho V^2 ScC_m \tag{18}$$

$$\dot{r} = \left(\frac{J_x - J_y}{J_z}\right)pq - \left(\frac{J_{xz}}{J_z}\right)qr + \frac{1}{2J_z}\rho V^2 SbC_n \tag{19}$$

$$\dot{V} = \frac{1}{m_x}\left(T \cos\beta(\cos\zeta \cos\alpha - \sin\zeta \sin\alpha)\right.$$
$$\left. - \frac{1}{2}\rho V^2 S(C_D \cos\beta - C_Y \sin\beta) - (mg - B)\sin\gamma\right) \tag{20}$$

$$\dot{\alpha} = q - \frac{1}{\cos\beta}\left\{((p\cos\alpha + r\sin\alpha)\sin\beta\right.$$
$$+ \frac{1}{Vm_z}(T \cos\zeta \sin\alpha + T \sin\zeta \cos\alpha$$
$$\left. + \frac{1}{2}\rho V^2 SC_L - (mg - B)\cos\mu \cos\gamma\right)\right\} \tag{21}$$

$$\dot{\beta} = (p \sin\alpha - r\cos\alpha) + \frac{1}{Vm_y}(-T\sin\beta(\cos\zeta\cos\alpha - \sin\zeta\sin\alpha)$$

$$+ \frac{1}{2}\rho V^2 S(C_Y \cos\beta + C_D \sin\beta) + (mg - B)\sin\mu\cos\gamma \Bigg) \qquad (22)$$

3 Direct Continuation Methodology for Constrained Dynamical Systems

The dynamics of most real-world systems could be captured by a set of ordinary nonlinear first order differential equations of form

$$\dot{x} = f(x, u) \qquad (23)$$

where $x \in \mathbb{R}^n$ is the state vector of n variables and $u \in \mathbb{R}^m$ is the control vector of m variables. For a six degrees-of-freedom aerial vehicles, state and control vectors are given by $x = [V, \alpha, \beta, p, q, r, \phi, \theta]^T \in \mathbb{R}^8$ and $u = [\eta, \delta_e, \delta_a, \delta_r]^T \in \mathbb{R}^4$, respectively. Dynamical stability evaluation of such a multi-input multi-output system using time simulation is ineffective. It would involve numerous combinations of control parameters with an infinite loop of initial condition dependency. Numerical continuation-based bifurcation methodology is an effective alternative to analyze such systems. This approach computes a series of steady states called equilibrium or trim solutions by simultaneously solving the algebraic equations for each control parameter by setting $\dot{x} = 0$ in Eq. (23). Stability of the system at each trim solution is also interpreted by calculating eigenvalues from its corresponding Jacobian matrix. Thus, characterizing the system locally gives a picture of global dynamics of the system.

The continuation approach solves Eq. (23) as a function of a single control parameter called continuation parameter, while retaining all other control parameters at a fixed value. The remaining control parameters called free variables could be tactically used to satisfy a set of constraints that defines a flight condition or maneuver. This is illustrated in Eq. (24), where $s \in u$ is the continuation parameter and $p \in u \in \mathbb{R}^3$ are free variables.

$$\dot{x} = f(x, s, p) \qquad (24)$$

This results in control schedules with respect to continuation parameter to satisfy the imposed constraints. It also helps in gauging the achievability of imposed constraints with the available control effort. It is notable that the number of constraint equations should not exceed $m - 1$ and free variables should have a significant influence on the constraint variables. Such constrained system analysis helps in the performance evaluation of maneuvers and in feasible maneuver design [11, 12]. A

recent development of direct continuation methodology for constrained system analysis [7] using MATCONT toolbox in MATLAB® substantially reduces the computational complexity and initial condition dependency. Thus, this methodology has been utilized to extend the capabilities of bifurcation-based continuation technique to trajectory design, feasibility evaluation, and optimization.

4 Maneuver Design with Feasibility Evaluation

This section evaluates different maneuvers for the autonomous operation of airship. At the operational altitude, airships may need to follow a straight level flight or exhibit turn maneuvers. Gauging the performance of turn maneuvers also helps in serving some of the major functionalities of airship like station-keeping. Besides analyzing the performance of airship at its pressure altitude, it is also important to assess its behavior during ascend and descend phases which are the challenging aspects of stratospheric airship platform. This section, therefore, evaluates the performance of airship in level, turn, ascend, and descend maneuvers. This section assumes neutral buoyancy and zero tilt angle for thrusters in level flight conditions.

4.1 Straight and Level Flight Maneuver

This section generates successive trim solutions for straight and level flight condition. These trims correspond to airship flying in straight line at pressure altitude with zero sideslip and wings level conditions. These conditions transcribe as constraint equations specified in Eq. (25).

$$\gamma = 0; \beta = 0; \phi = 0 \tag{25}$$

These three constraints are satisfied by freeing three control variables. Control variables to be freed should be appropriately chosen such that they have substantial effect on constraints. In this case, η, δ_r, and δ_a are freed to satisfy constraints on γ, β, and ϕ, respectively. In the bifurcation plots in Fig. 3, solid lines represent stable trim solutions and dotted lines correspond to unstable trim solutions. Thus, it could be inferred that Hopf bifurcation occurs at the state and control trim vectors specified in Eqs. (26) and (27), respectively, with velocity in m/s and angles in degrees. The instability is caused due to divergence of pendulum mode at higher velocities.

$$x = [15.7686, \, -0.3912, 0, 0, 0, 0, 0, \, -0.3912]^{\mathrm{T}} \tag{26}$$

$$\eta = 0.2307, \delta_e = 1.0657, \delta_a = 0, \delta_r = 0 \tag{27}$$
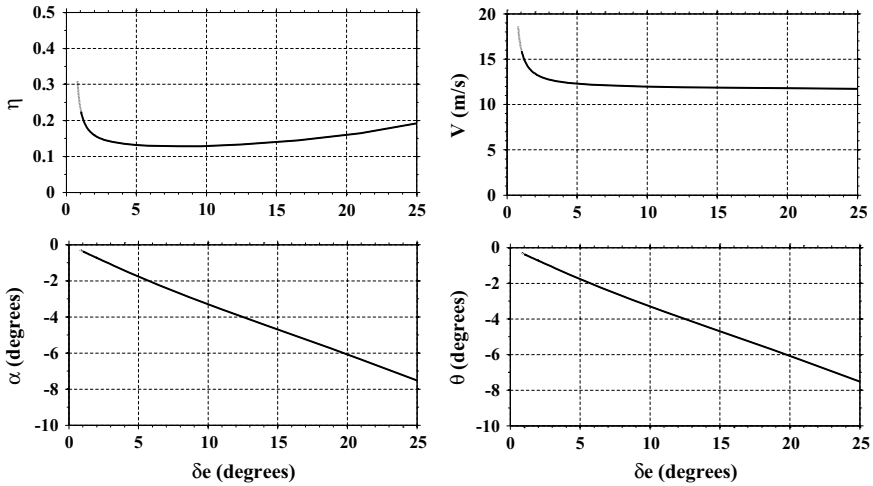
Fig. 3 Bifurcation plots for straight and level flight maneuver

Airship is an underactuated system with eight state variables and four control variables. Thus, choosing a stable trim as a maneuver design criterion helps in maintaining the integrity of the system even in the presence of parametric and nonparametric uncertainties. These set of trim solutions also help in selecting an optimal maneuver considering the complete dynamics of the system. For example, from the bifurcation plots, minimum energy straight and level flight maneuver corresponds to $\eta = 0.128$ and $\delta_e = 7.5°$, whereas minimum time straight and level flight maneuver corresponds to $\eta = 0.23$ and $\delta_e = 1.05°$. Thus, based on the applicability desired maneuver could be chosen from a set of stable trim solutions.

4.2 Level Turn Maneuver

Most of the studies on aircraft turn performance consider zero-sideslip bank-to-turn maneuvers. But in contrary, attainable bank angle computed from standard bifurcation analysis for maximum aileron deflection is only about $\pm 5°$, whereas skid angle for maximum rudder deflection is $\pm 30°$ which makes skid-to-turn an effective alternative for airships. The inherent limitation of roll in airship is also evident from [13] where roll angle is limited to $\pm 5°$ and [14] ignores roll from airship equations of motion. This is typically attributed to the dependency of airship on buoyancy for lifting as dynamic lift force is less. In addition, location of center of buoyancy is above the center of gravity which nullifies the moment about the roll axis [14]. This ascribes as an advantage on the functionality of airship, as payload for various applications is usually earth-pointing. Thus, this paper deals with level skid-to-turn maneuver design and evaluation for airship. On corollary, performance evaluation of

turn maneuvers also results in an effective hover control strategy. Most applications of airship demand hovering at a stationary position coordinate. Airship is neutrally stable at hover condition, thereby making hover stabilization an important aspect of its control design.

The constraint equations for the evaluation of turn maneuvers are chosen prudently, such that the constraints are achievable by the available control capabilities. As sideslip angle corresponding to maximum rudder deflection is $\pm 30°$, sideslip angle of $-25°$ with zero flight path and roll angle are considered for illustration. This choice of higher sideslip angle could help in characterizing the performance of airship by evaluating its maximum possible turn rate and minimum possible turn radius. Thus

$$\gamma = 0; \beta = -25°; \phi = 0 \tag{28}$$

As in straight and level flight maneuver, η, δ_r, and δ_a are freed to satisfy constraints on γ, β, and ϕ, respectively. As inferred from the bifurcation plots in Fig. 4, Hopf bifurcation occurs at the state and control trim vectors specified in Eqs. (29) and (30), respectively, with velocity in m/s and angles in degrees. But this trim corresponds to enforced throttle ratio of 1.2253, which an airship is incapable of achieving as the required thrust is more than the maximum available thrust. The onset of this instability is characterized by the pendulum mode becoming unstable at higher velocities.

$$\boldsymbol{x} = [16.5822, -1.6291, -25, 0.0320, 0, 1.1248, 0, -1.6291]^T \tag{29}$$

$$\eta = 1.2253, \delta_e = 5.4214, \delta_a = -3.3578, \delta_r = -19.5993 \tag{30}$$

In Fig. 5, turn rate (ω) is computed by solving rotational kinematic equation of yaw rate $(\dot{\psi})$ [Eq. (9)] and turn radius (R) is obtained by dividing velocity of the airship by turn rate, i.e., $R = V/\omega$. On thorough perusal of Figs. 4 and 5, it could be inferred that the maximum possible fastest turn and minimum possible tightest turn corresponds to elevator deflection of about $20°$, with consideration on state and control limitations (δ_r reaches its saturation limit nearly after $\delta_e = 20°$). Thus, maximum turn rate and minimum turn radius are approximately $1°$/s and 730 m, respectively. It is also noteworthy that the tightest turn demands comparatively a higher thrust.

4.3   Ascend and Descend Maneuvers

This section formulates feasible ascend and descend trajectories, emphasizing lateral excursions minimization with considerations on state and control constraints. The buoyant force experienced by the airship is given by
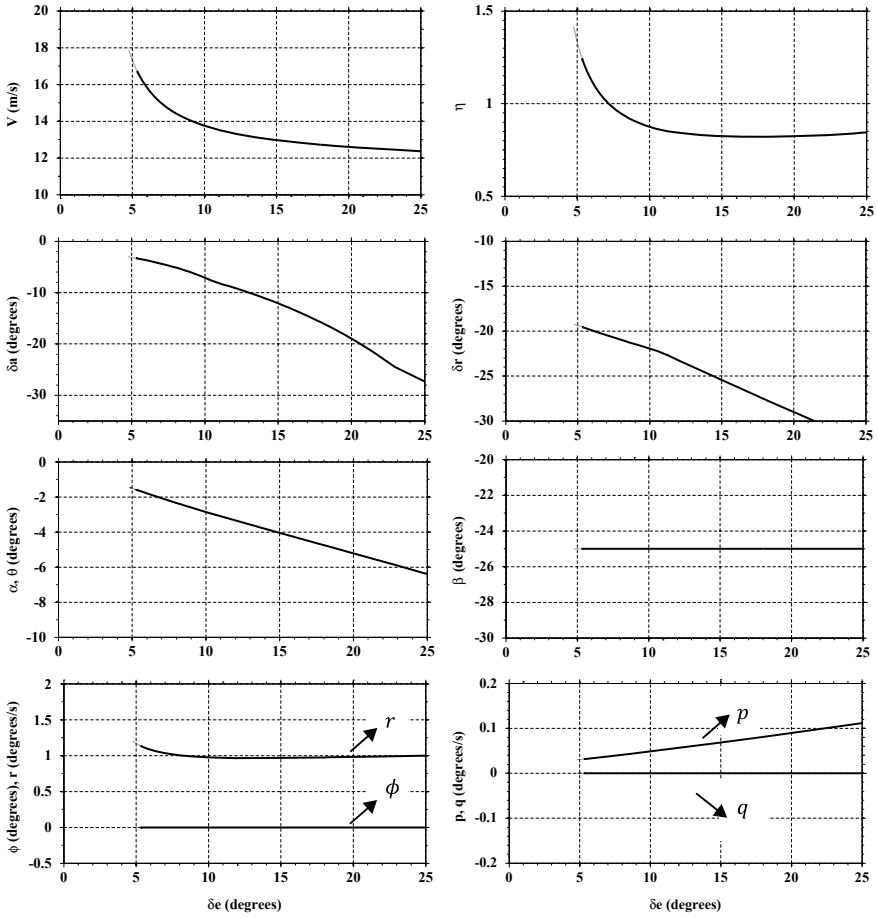
Fig. 4 Bifurcation plots for level turn maneuver
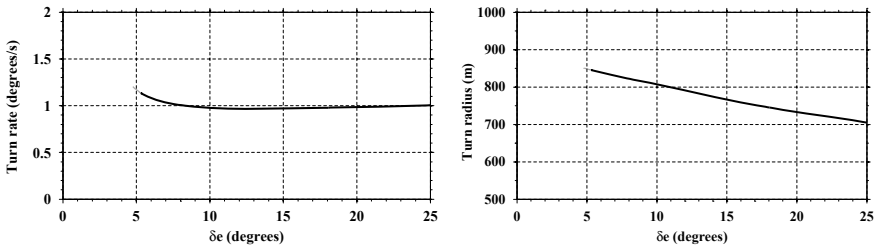
Fig. 5 Performance of level turn maneuver

$$B = U(h)\rho(h) \tag{31}$$

where U is the volume of the body and ρ is the mean density of air surrounding the body. The envelope of airship could handle only small differential pressure. Internal pressure is regulated using ballonet system to maintain zero static lift, i.e., $B = W$ throughout the flight regime. Airship is considered an open system with ballonets open to the atmosphere. Thus, change in ballonet's volume during ascend and descend changes the volume of the system with the mass of airship remaining constant.

Airship employing thrust vectoring exhibit enhanced ascend and descend performance. Thus, the vector angle for ascend is taken as 45°, based on exhaustive flight testing performed on the Airship Industries Skyship 500/600 series [8]. To achieve a minimum time ascend, maximum flight path angle and maximum available power, P_m is utilized. With the assumption that the propeller and motor efficiency is 1, maximum available thrust, T_m is given by

$$T_\mathrm{m} = P_\mathrm{m}/V \tag{32}$$

The constraints for minimum time ascend is given by

$$\gamma = 10°; \beta = 0; \phi = 0; \eta = 1; \zeta = 45° \tag{33}$$

During ascend, ρ has a nonlinear variation with respect to the body's altitude. This variation affects the dynamic pressure of airship which in turn affects the aerodynamic forces and moments. Thus, change in ρ is adapted by inducing it in control vector and using it as a continuation parameter. For the constraints specified in Eq. (33), δ_e, δ_a, and δ_r are freed. Since, constraints on lateral directional variables are zero, trim values of lateral directional controls, δ_a and δ_r are zero, thus, p and r are as well zero. Elevator control schedule with maximum available thrust and longitudinal state variables are plotted in Fig. 6. It could be inferred that the Hopf bifurcation occurs at the state and control trim vectors specified in Eqs. (34) and (35), respectively, with density in kg/m^3, velocity in m/s, and angles in degrees.

$$\boldsymbol{x} = [16.6446, 1.3431, 0, 0, 0, 0, 0, 11.3926]^T \tag{34}$$

$$\eta = 1, \zeta = 45, \delta_e = -12.3505, \delta_a = 0, \delta_r = 0, \rho = 0.1557 \tag{35}$$

This minimal time ascend maneuver demands a substantial lateral air space of around 100 km, which is difficult to ensure in the air traffic zone. The lateral excursion is largely reduced by imparting a skid angle, which results in a helical ascend trajectory with radius of helix corresponding to the induced skid angle. A larger skid angle reduces the radius of turn but it must be ensured that the proposed skid angle is achievable by the available control efforts. For helical ascend maneuver, constraints are chosen as
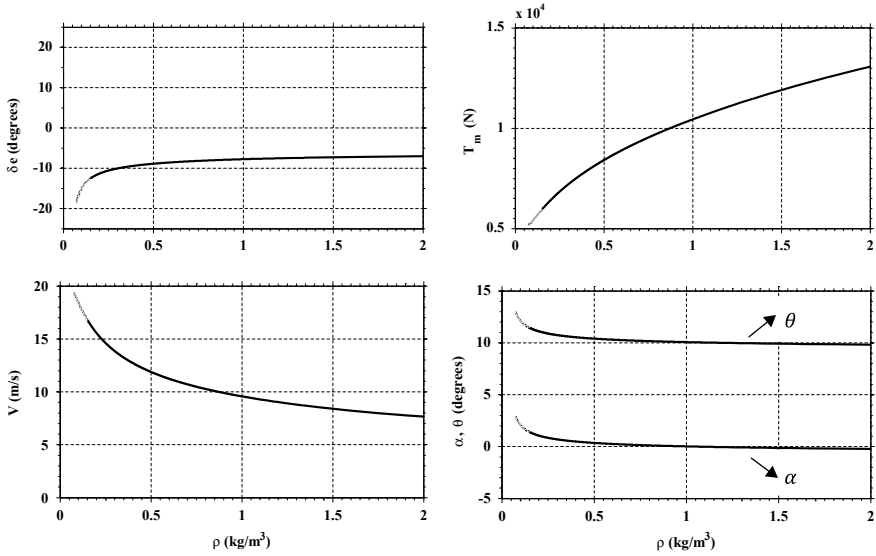
Fig. 6 Response for minimal time ascend

$$\gamma = 10°; \beta = 5°; \phi = 0; \eta = 1; \zeta = 45° \tag{36}$$

Control schedules and the response of state variables for the considered helical ascend are plotted in Figs. 7 and 8. Hopf bifurcation occurs at the state and control trim vectors specified in Eqs. (37) and (38), respectively, with density in kg/m^3, velocity in m/s, and angles in degrees.

$$\mathbf{x} = [16.0369, 1.4108, 5, 0.0652, 0, -0.3203, 0, 11.4991]^T \tag{37}$$

$$\eta = 1, \zeta = 45, \delta_e = -13.7454, \delta_a = 0.4804, \delta_r = 7.0004, \rho = 0.1550 \tag{38}$$

Both minimal time and helical ascend maneuvers with $\zeta = 45°$ and $\eta = 1$ become unstable at a density of around 0.15. This corresponds to an altitude of about 16,670 m, which is conveniently above the air traffic zone and other intrusions. Velocity also shoots up to its maximum allowable value. This demands a change in approach to ensure the stability of airship after the airship reaches an altitude of 16,670 m.

Minimal lateral excursion need not be considered a hard constraint above an altitude of 16,670 m, aiding zero skid angle consideration. Exerting maximum available thrust during ascend increases the velocity of airship as inferred from Figs. 6 and 8. This calls for curbing the velocity below its maximum value to ensure safety. Thus, a constraint in velocity of 13.5 m/s is considered with $\gamma = 3°$. The tilt angle is brought back to zero. This results in the constraint equations given by
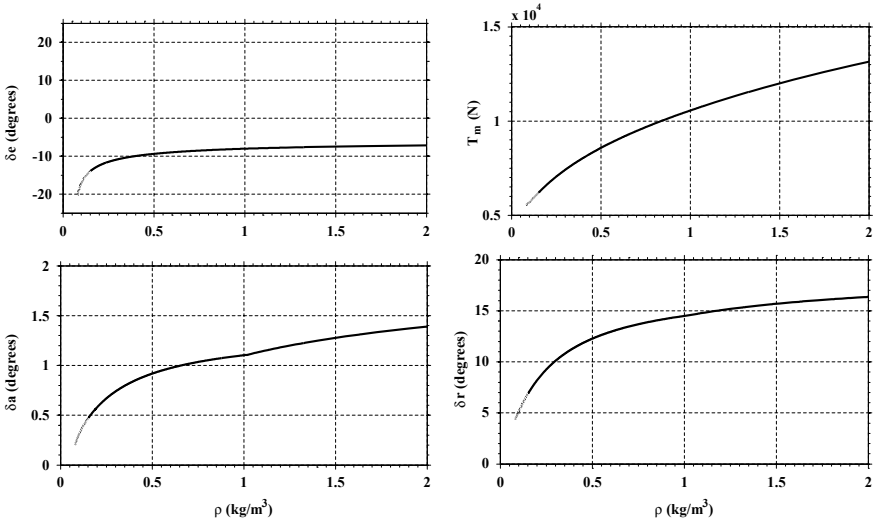
Fig. 7 Control schedule for helical ascend
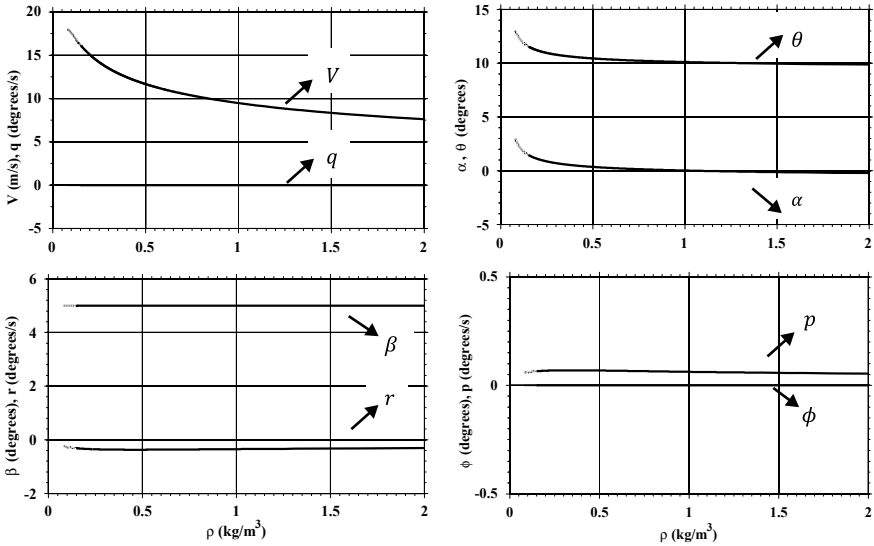
Fig. 8 Response of state variables for helical ascend

$$V = 13.5 \, \text{m/s}; \; \gamma = 3°; \; \beta = 0; \; \phi = 0; \; \zeta = 0 \qquad (39)$$

η and δ_e are freed to achieve constraints on V and γ with the maximum available thrust taken to be 6000 N. It is also evident that δ_a and δ_r are zero to achieve zero skid and roll angle. Response of non-zero state and control variables with respect to
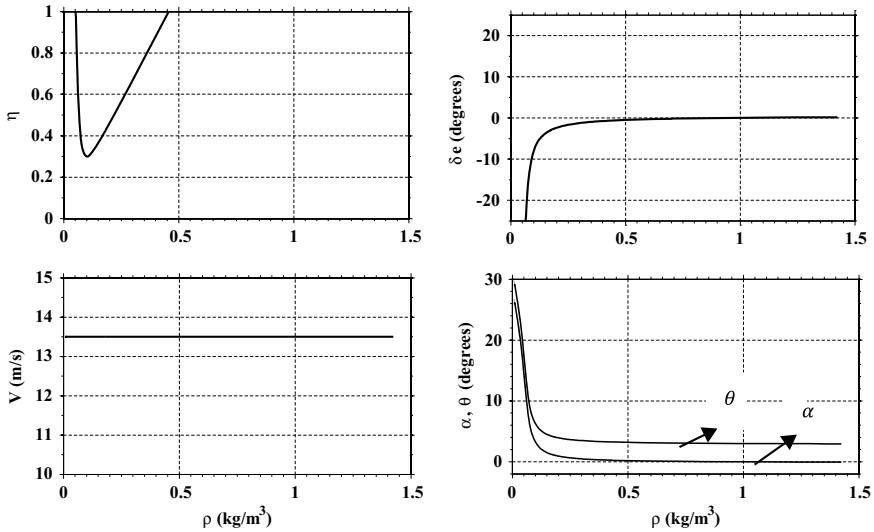
Fig. 9 Response for longitudinal only maneuver with constraints on V and γ

the specified set of constraints is depicted in Fig. 9. From the plots, it is inferred that the flight path angle is maintained at $3°$ and the commanded velocity is unachievable for densities above $0.45 \, \text{kg/m}^3$, as throttle ratio shoots above 1. Thus, for velocity constraint maneuver during ascend, velocity should be judiciously chosen through thorough perusal on velocity profile corresponding to maximum available thrust in Fig. 6. This maneuver could be used in the final neck of ascend, beyond the air traffic prone zone of the lower stratosphere.

The same approach could be carried out for descend maneuvers design. While descending, constrained longitudinal only maneuver with $V = 13.5 \, \text{m/s}$ and $\gamma = -3°$ is used till an altitude of $16 \, \text{km}$. After which, a helical descend maneuver with $\gamma = -10°$ is employed. A narrow regime of stability in ascend and descend maneuver design emphasizes the importance of the proposed maneuver design approach. A randomly chosen maneuver might not work under the state and control constraints of airship. This explains scant attention on ascend and descend in the literature pertaining to the control of stratospheric airship.

5 Validation

This section illustrates the feasibility of proposed maneuvers with control schedules in open-loop. It also helps in analyzing the performance of computational bifurcation methodology in maneuver design and optimization approaches.

5.1 Level Performance Analysis

A scenario of executing the tightest possible turn from a steady level flight condition is considered. A feasible state and control trim corresponding to a stable straight and level condition is chosen from Fig. 3 and is tabulated in Eqs. (40) and (41), respectively, with velocity in m/s and angles in degrees.

$$x = [14.6671, \ -0.4810, 0, 0, 0, 0, 0, \ -0.4810]^T \tag{40}$$

$$\eta = 0.1913, \delta_e = 1.3145, \delta_a = 0, \delta_r = 0 \tag{41}$$

Airship is simulated with controls in Eq. (41) for 500 s. After which it is commanded to execute the minimum radius turn maneuver. From Fig. 4, state and control trim corresponding to a stable and achievable minimum radius of turn is chosen and is given in Eqs. (42) and (43), respectively, with velocity in m/s and angles in degrees.

$$x = [12.7204, \ -4.7627, \ -25, 0.0812, 0, 0.9750, 0, \ -4.7627]^T \tag{42}$$

$$\eta = 0.8216, \delta_e = 18.0558, \delta_a = -15.9716, \delta_r = -27.6369 \tag{43}$$

Response of airship during the execution of proposed maneuver is plotted in Figs. 10 and 11. For the initial 500 s, airship travels with the velocity of about 14.6 m/s covering a distance of 7300 m. Airship is then commanded to execute level turn maneuver with minimum possible turn radius. It is inferred from Fig. 10 that the radius of turn is approximately 740 m, which matches with the turn radius computed and plotted in Fig. 5. In order to maintain zero flight path angle, η is freed as discussed in Sect. 4. But controlling γ demands controlling both α and θ, i.e., two state variables are controlled using a single control input. Such issues of underactuation are effectively handled by this maneuver design approach.

This illustration also helps in analyzing the hover capabilities of airship. Hover of airship at the pressure altitude is a neutrally stable flight condition [15]. Thus,
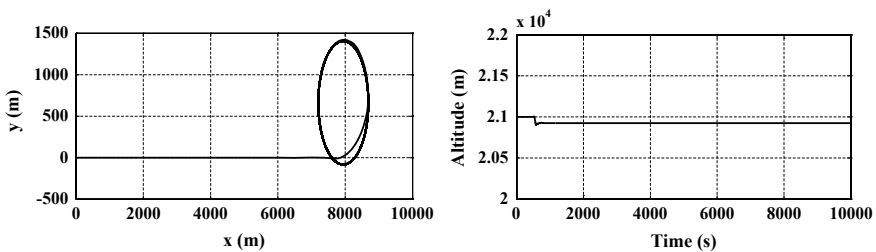
Fig. 10 Position trajectories for the considered maneuver
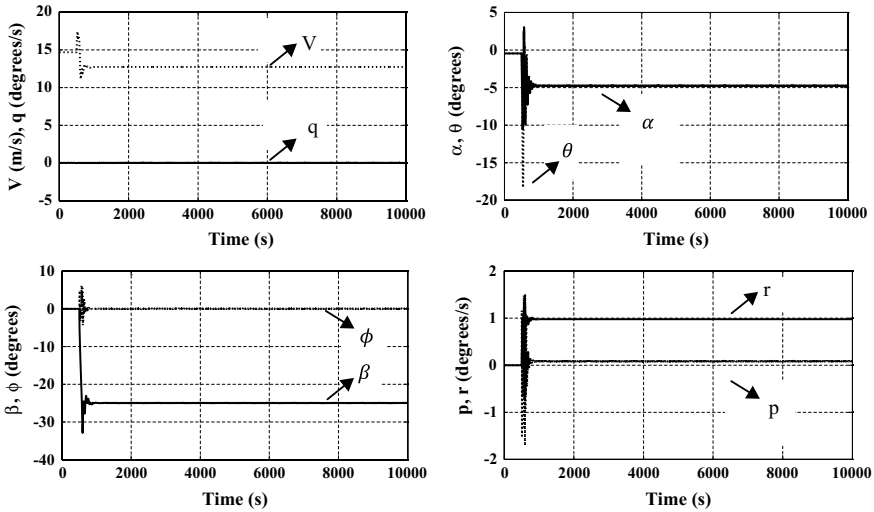
Fig. 11 Response of state variables for the considered maneuvers

maintaining its position coordinates amidst strong gust becomes a challenging task in autonomous airship maneuvering. Few works demonstrate the challenges faced by airship during hover in turbulent atmospheric environments and infer that significant thrust and control power are required to station-keep [16, 17], with the risk on system's integrity at worst case scenarios. In such situations, the proposed tightest turn maneuver could be commanded with the backing of robust controller to achieve it. This causes airship to suffer only a minor change from the station-kept position coordinates. If the thrust demand shoots up further, skid angle could be considerably reduced and maneuver is appropriately redesigned while ensuring the safety and integrity of the airship.

5.2 Ascend Maneuver Evaluation

The feasibility of proposed ascend maneuvers with control schedules in open-loop is evaluated. The proposed helical and longitudinal only ascend maneuvers are evaluated using the simulation framework portrayed in Fig. 12. Based on the altitude of airship ($h = -z_E$), ρ is calculated using curve fitting of atmospheric density and altitude data. From sea level corresponding to $\rho = 1.2256\,\text{kg/m}^3$, through $h = 16,670\,\text{m}$ corresponding to $\rho = 0.15$, control schedules of helical ascend with respect to their corresponding densities (plotted in Fig. 7) are fed to airship model with $\eta = 1$ and $\zeta = 45°$. Subsequently, control schedules corresponding to longitudinal only ascend (plotted in Fig. 9) with $V = 13.5\,\text{m/s}$ and $\gamma = 3°$ are fed, with $T_m = 6000\,\text{N}$ and $\delta_a, \delta_r, \zeta = 0$, till the airship reaches its operational altitude
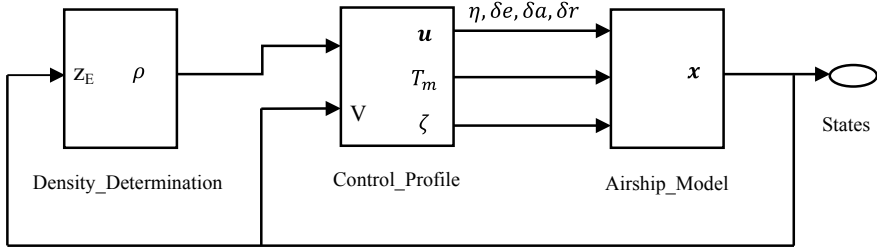
Fig. 12 Simulation framework for ascend maneuver validation
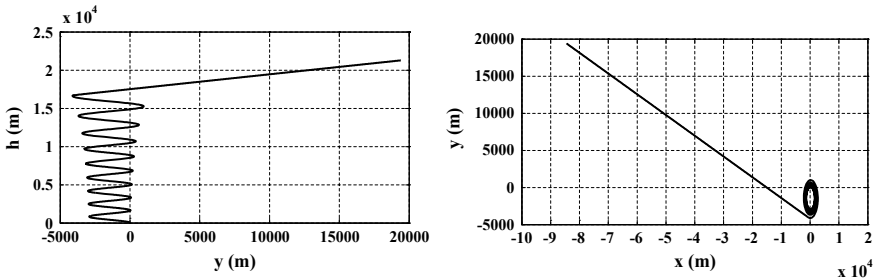
Fig. 13 Position trajectories for the proposed ascend maneuver

corresponding to density of around $0.075 \, \text{kg/m}^3$. The response of state variables $\boldsymbol{x} = [V, \alpha, \beta, p, q, r, \phi, \theta, \psi, x_E, y_E, z_E]^T$ is recorded and fed back to determine corresponding density and control profile.

Position trajectories and state response of the implemented ascend maneuver are plotted in Figs. 13 and 14. It is evident that the helical ascend with $\gamma = 10°$ is carried out till an altitude of 16,500 m. During this phase, β is maintained at 5° to limit lateral excursion to a maximum of 5000 m, as inferred from Figs. 13 and 14. This is beneficial while climbing through air traffic and tropospheric interferences. Beyond this altitude, longitudinal only maneuver with constraints on V and γ is executed. The feasibility of the proposed ascend maneuver is thus successfully validated.

6 Conclusions

Autonomous maneuvering of aerial vehicles has gained predominant interest in the recent past. In that regard, one of the prime realms that receive scant emphasis is maneuver design. This work establishes an effective maneuver design technique using bifurcation-based continuation approach. This methodology takes into consideration the dynamics of the system with state and control constraints and generates a series of feasible solutions. A few major challenges in airship autonomy like stability
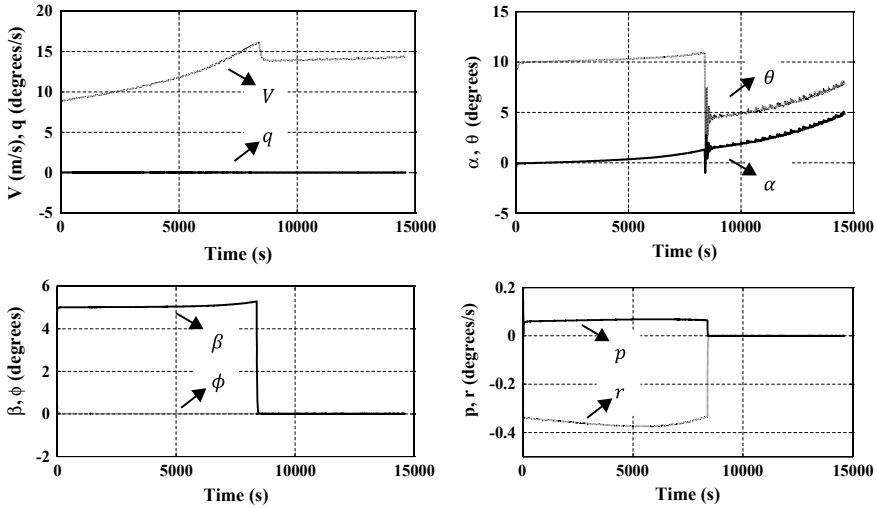
Fig. 14 Response of state variables for the proposed ascend maneuvers

during hover, ascend, and descend phases are addressed. The proposed maneuvers are then validated using an open-loop formulation with computed control profiles from bifurcation analysis. The flexibility to choose from a family of feasible solutions with different constraint sets makes this a unique platform for maneuver design. The reliability of controllers in uncertain environments could be greatly enhanced with the knowledge of feasible solutions, especially for underactuated systems.

References

1. Tsiotras P, Mesbahi M (2017) Toward an algorithmic control theory. J Guid Control Dyn 40(2):194–196
2. Lu P (2017) Introducing computational guidance and control. J Guid Control Dyn 40(2):193
3. Hima S, Bestaoui Y (2002) Motion generation on trim trajectories for an autonomous underactuated airship. In: Proceedings of the 4th international airship convention and exhibition, airship association, Cambridge, England
4. Repoulias F, Papadopoulos E (2007) Dynamically feasible trajectory and open-loop control design for unmanned airships. In: Proceedings of the 8th IFAC symposium on robot control, Vol 39, no 15, pp 592–597
5. Khatri AK, Singh J, Sinha NK (2012) Aircraft maneuver design using bifurcation analysis and sliding mode control techniques. J Guid Control Dyn 35(5):1435–1449
6. Dhooge A, Govaerts W, Kuznetsov AY (2003) MATCONT: A MATLAB package for numerical bifurcation analysis of ODEs. ACM Trans Math Softw 29(2):141–164
7. Vora AS, Sinha NK (2017) Direct methodology for constrained system analysis with applications to aircraft dynamics. J Aircr 54(6):2378–2385
8. Khoury GA (2012) Airship technology. Cambridge University Press, New York, USA

9. Rana V, Ajith K, Sinha NK, Amiatbha P, Sati SC (2015) Configuration analysis of stratospheric airship. In: Symposium on applied aerodynamics and design of aerospace vehicles, VSSC, Thiruvananthapuram, India
10. Sinha NK, Ananthkrishnan N (2014) Elementary flight dynamics with an introduction to bifurcation and continuation methods. CRC Press, Boca Raton, USA
11. Ananthkrishnan N, Sinha NK (2001) Level flight trim and stability analysis using extended bifurcation and continuation method. J Guid Control Dyn 24(6):1225–1228
12. Khatri AK, Singh J, Sinha NK (2013) Accessible regions for controlled aircraft maneuvering. J Guid Control Dyn 36(6):1829–1834
13. Lee S, Bang H (2007) Three-dimensional ascent trajectory optimization for stratospheric airship platforms in the jet stream. J Guid Control Dyn 30(5):1341–1351
14. Mueller JB, Zhao YJ, Garrard WL (2009) Optimal ascent trajectories for stratospheric airships using wind energy. J Guid Control Dyn 32(4):1232–1245
15. Cook MV, Lipscombe JM, Goineau F (2000) Analysis of the stability modes of the non-rigid airship. Aeronaut J 104(1036):279–290
16. Schmidt DK (2007) Modeling and near-space stationkeeping control of a large high-altitude airship. J Guid Control Dyn 30(2):540–547
17. Schmidt DK, Stevens J, Roney J (2007) Near-space station-keeping performance of a large high-altitude notional airship. J Aircr 44(2):611–615